Magnesium Alloys: Metallographic Techniques and Microstructures
Revised by Kenneth J. Clark, Wellman Dynamics Corp.

<Previous section in this article

Atlas of Microstructures for Magnesium Alloys

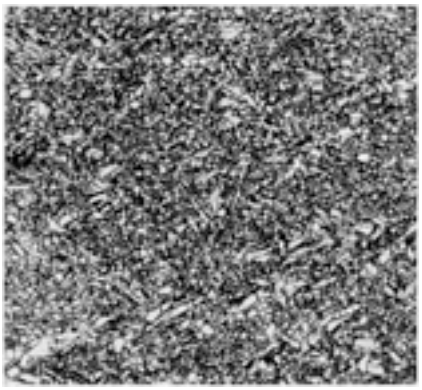

Fig. 1 Alloy AZ31B-H24 sheet. Longitudinal edge view of worked structure, showing elongated grains, and mechanical twins, which resulted from warm rolling of the sheet. Etchant 8, Table 1. 250×

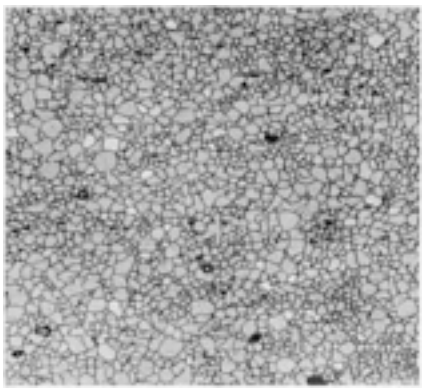

Fig. 2 Alloy AZ31B-O sheet. Longitudinal edge view of structure recrystallized by annealing. Particles of manganese-aluminum compound (dark gray) and fragmented $Mg_{17}Al_{12}$ (outlined). Etchant 8, Table 1. 200×

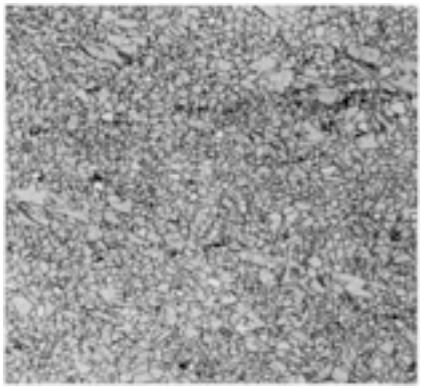

Fig. 3 Alloy AZ31B tooling plate. Longitudinal edge view. Essentially recrystallized structure resulting from anneal flattening; outlined particles of fragmented $Mg_{17}Al_{12}$. Etchant 8, Table 1. 200×

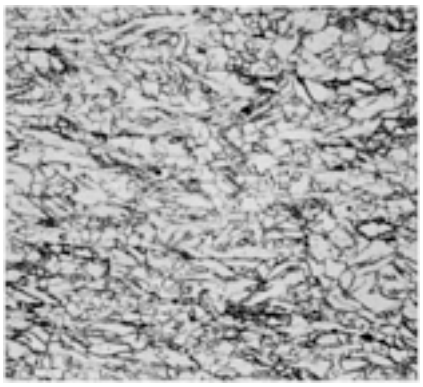

Fig. 4 ZE10A-H24 sheet. Longitudinal edge view of worked structure similar to that in Fig. 1, showing elongated grains and mechanical twins (bounded by parallel lines), resulting from warm rolling of the sheet. Etchant 7, Table 1. 500×

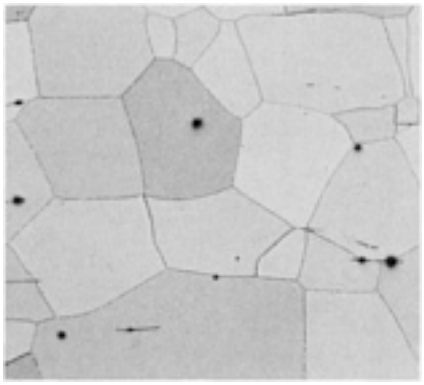

Fig. 5 LA141A-O sheet. Longitudinal edge view of recrystallized structure that resulted from annealing for 30 min at 260 °C (500 °F). The structure is generally clean, but entrapped dross is present in some areas. Etchant 5, Table 1.250×

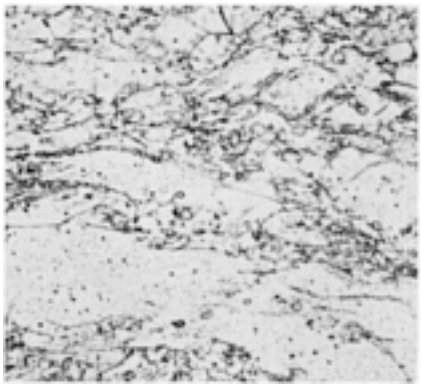

Fig. 6 HM21A-T8 sheet. Longitudinal edge view of worked structure, showing Mg_4Th, both as outlined particles of fragmented massive compound and as precipitate within grains and at boundaries of the elongated grains. Etchant 5, Table 1. 500×

[graphic]

Fig. 7 HK31A-H24 sheet. Longitudinal edge view, showing structure similar to Fig. 6, but with less Mg_4Th precipitated in grains and more at the elongated grain boundaries. Etchant 5, Table 1. 500×

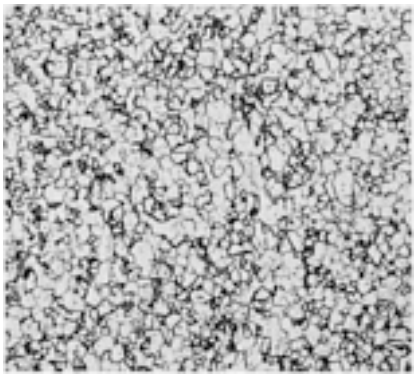

Fig. 8 HK31A-O sheet. Longitudinal edge view of structure recrystallized by annealing. Note that most of the Mg_4Th precipitate shown in Fig. 7 has redissolved. See also Fig. 9. Etchant 5, Table 1, 10 s. 250×

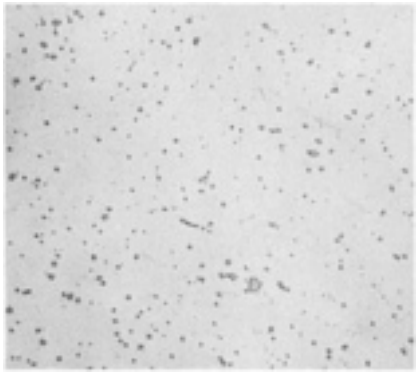

Fig. 9 HK31A-O sheet. Same as Fig. 8, except not etched, which has made the outlined particles of fragmented massive Mg_4Th compound more easily visible. As-polished. 500×

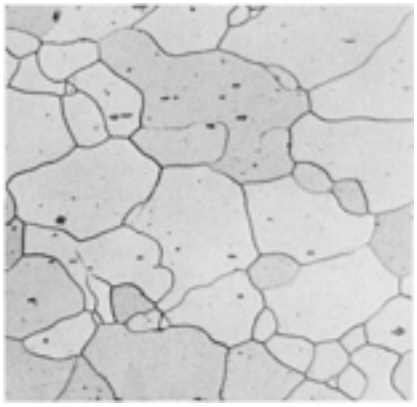

Fig. 10 AZ31 B-F extrusion. Longitudinal view of hot-worked structure. Large, equiaxed recrystallized grains; particles of manganese-aluminum compound and fragmented $Mg_{17}Al_{12}$. Etchant 8, Table 1. 250×

Fig. 11 AZ61A-F extrusion. Longitudinal view of hot-worked structure. Small, equiaxed recrystallized grains; stringers of fragmented $Mg_{17}Al_{12}$. See also Fig. 12. Etchant 6, Table 1. 250×

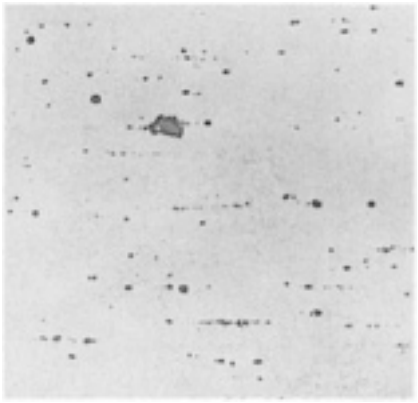

Fig. 12 Same as Fig. 11, except this specimen has not been etched, making the stringers of fragmented $Mg_{17}Al_{12}$more easily visible. As-polished. 250×

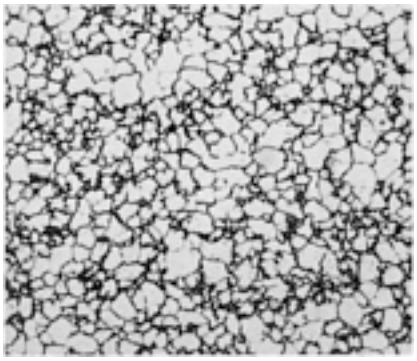

Fig. 13 AZ80A-F extrusion. Longitudinal view of hot-worked structure. Small, equiaxed recrystallized grains; small amount of $Mg_{17}Al_{12}$ discontinuous precipitate at the grain boundaries. See also Fig. 14. Etchant 3, Table 1, 15 s. 250×

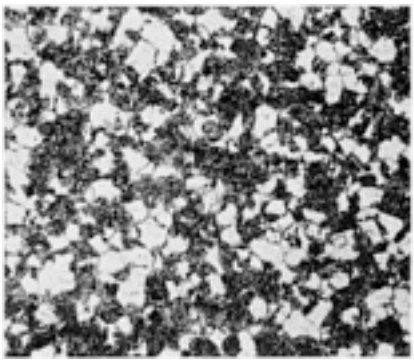

Fig. 14 AZ80A-T5 extrusion. Longitudinal view showing much mottled $Mg_{17}Al_{12}$ discontinuous precipitate near the grain boundaries, resulting from the artificial aging treatment. Compare with Fig. 13. Etchant 2, Table 1, 5 s. 250×

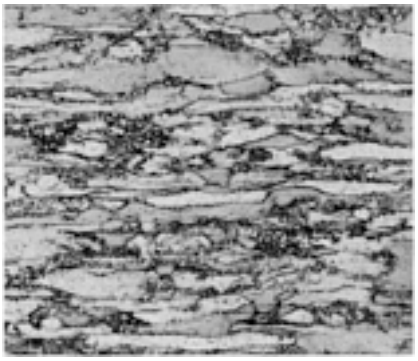

Fig. 15 ZK21A-F extrusion. Longitudinal view of hot-worked structure. Small equiaxed recrystallized grains at the boundaries of and also within large, unrecrystallized elongated grains. Etchant 6, Table 1. 100×

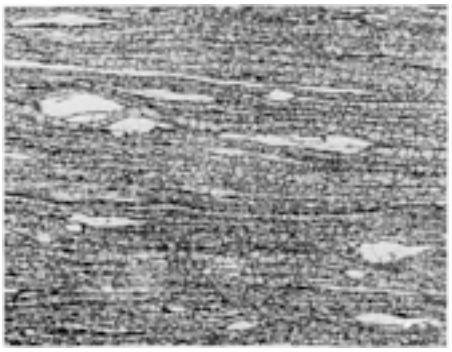

Fig. 16 ZK60A-F extrusion. Longitudinal view of banded hot-worked structure. Small, recrystallized grains; light islands are solid solution deficient in zinc and zirconium (due to alloy segregation) and so more resistant to hot working. See also Fig. 17. Etchant 6, Table 1, then Etchant 4, Table 1. 250×

[graphic]

Fig. 17 Same as Fig. 16, except artificially aged to the T5 temper. Despite higher magnification,

structure appears same as Fig. 16 (precipitate formed during aging is unresolvable by microscopy). Etchant 7, Table 1, 7 s, then Etchant 6, Table 1, 1 s. 500×

Fig. 18 HM31A-T5 extrusion. Longitudinal view of banded hot-worked structure. Small, recrystallized grains; dark Mg_4Th grain-boundary precipitate; light islands are solid solution rich in thorium and so more resistant to hot working; gray particle is manganese. Etchant 5, Table 1. 500×

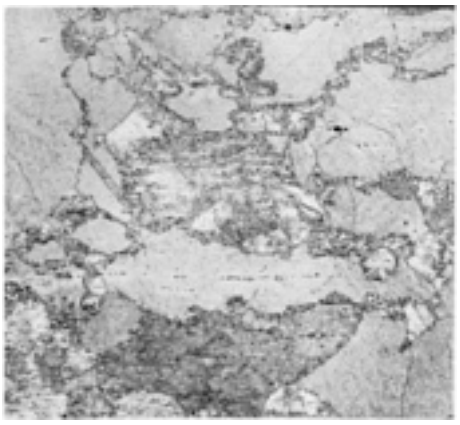

Fig. 19 AZ80A-T5 forging. Longitudinal view of hot-worked structure, showing large, recrystallized grains and spheroidized $Mg_{17}Al_{12}$ discontinuous precipitate mainly in the grains near the boundaries. Etchant 5, Table 1. 200×

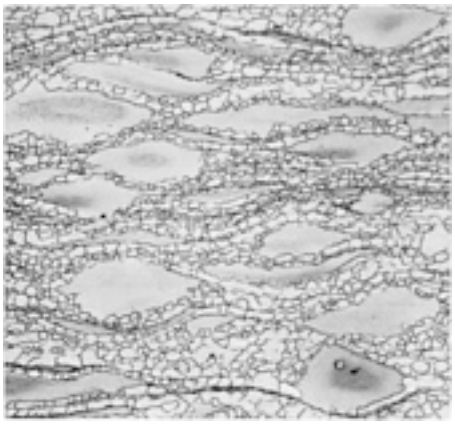

Fig. 20 ZK60A-T5 forging. Longitudinal view. Structure same as Fig. 17, but with slightly larger grains and increased alloy segregation. Etchant 7, Table 1, 7 s, then Etchant 6, Table 1, 2 s. 500×

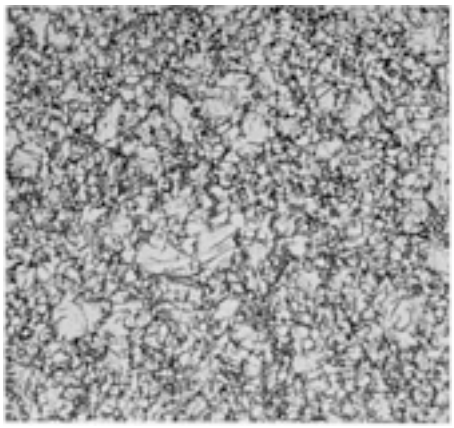

Fig. 21 HM21A-T5 forging. Longitudinal view. Structure is similar to that of sheet shown in Fig. 6, except the forging has smaller grains. (Grain growth in sheet caused by solution heat treatment.) Etchant 5, Table 1. 250×

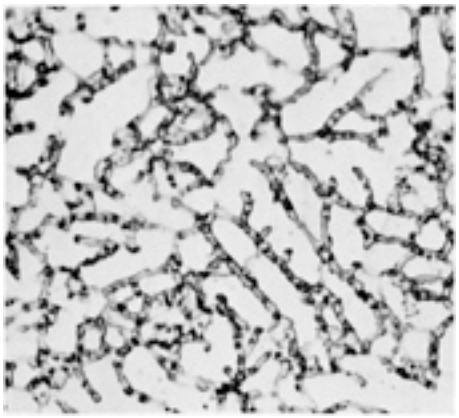

Fig. 22 AM60A-F die casting. Small, cored grains of magnesium solid solution in which the aluminum content increases toward the boundaries; passive $Mg_{17}Al_{12}$ compound at grain boundaries. Relief polishing causes dark areas. See also Fig. 23. Etchant 3, Table 1. 500×

[graphic]

Fig. 23 AS41A-F die casting. Same structure as that shown in Fig. 22, but with the addition of Mg_2Si in Chinese script and globular forms. Etchant 3, Table 1, 5 s. 500×

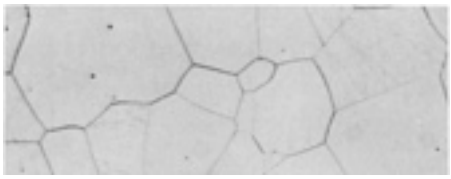

Fig. 24 K1A-F die casting. Small crystals of zirconium randomly dispersed in grains of magnesium that are larger than those in more highly alloyed die castings (compare with Fig. 22, 23, and 25.) Etchant 2, Table 1, 10 s. 250×

[graphic]

Fig. 25 AZ91A-F die casting. Massive $Mg_{17}Al_{12}$ compound at the boundaries of small, cored grains. Segregation (coring) in the grains and absence of precipitated discontinuous $Mg_{17}Al_{12}$ are results of the rapid cooling rate of die castings. See also Fig. 26 and 27. Etchant 2, Table 1, 5 s. 500×

[graphic]

Fig. 26 AZ92A-F permanent mold casting. $Mg_{17}Al_{12}$ compound: massive (outlined) at grain boundaries; precipitated (dark) near grain boundaries. Slower cooling rate than that of die castings has resulted in larger grains than in structure shown in Fig. 25. Etchant 2, Table 1, 5 s. 250×

[graphic]

Fig. 27 AZ92A-F sand casting. Same microstructure as that shown in Fig. 26, except the slower cooling rate, in comparison with that of permanent mold castings, has resulted in larger grains. See

Fig. 32 for effects of aging. Etchant 2, Table 1, 5 s. 250×

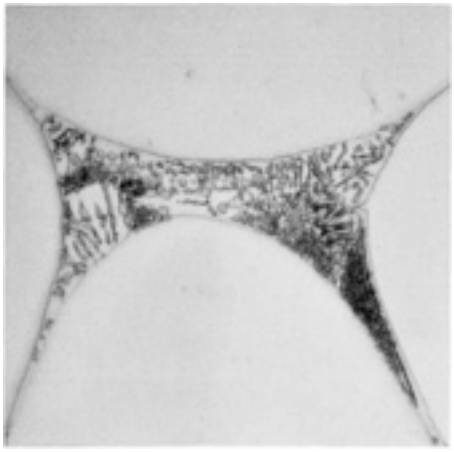

Fig. 28 AZ92A-F sand casting. The appearance of the interdendritic eutectic, a mixture of magnesium solid solution and $Mg_{17}Al_{12}$, was retained in this form by a rapid quench from above the eutectic temperature. See also Fig. 29. Etchant 2, Table 1, 5 s. 1500×

[graphic]

Fig. 29 AM100A-F, as-cast. Massive $Mg_{17}Al_{12}$ compound containing globular magnesium solid solution and surrounded by lamellar $Mg_{17}Al_{12}$ precipitate. Normal air cooling produces this type of segregated eutectic. Compare with Fig. 28 and 30. Etchant 2, Table 1, 5 s. 500×

Fig. 30 AZ92A-F, as-cast. Massive $Mg_{17}Al_{12}$ compound surrounded by lamellar $Mg_{17}Al_{12}$ precipitate. Normal air cooling of zinc-containing magnesium-aluminum alloys produces this type of completely divorced eutectic. Compare with Fig. 29. Etchant 2, Table 1. 500×

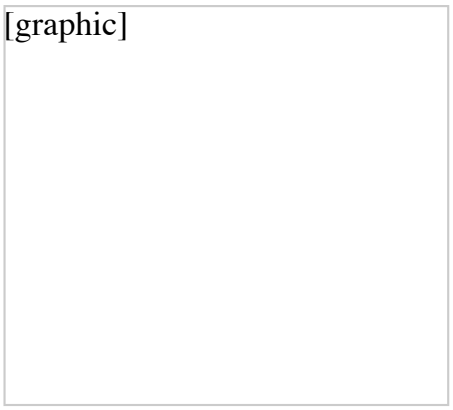

Fig. 31 Massive $Mg_{32}(Al,Zn)_{49}$ (white) in as-cast alloy AZ63A-F. Specimen etched with 50% picral to protect Mg_2Si (hexagonal particle) from HF, then with 5% HF to blacken $Mg_{17}Al_{12}$ and distinguish it from $Mg_{32}(Al,Zn)_{49}$, then with 10% picral to darken the matrix. 500×

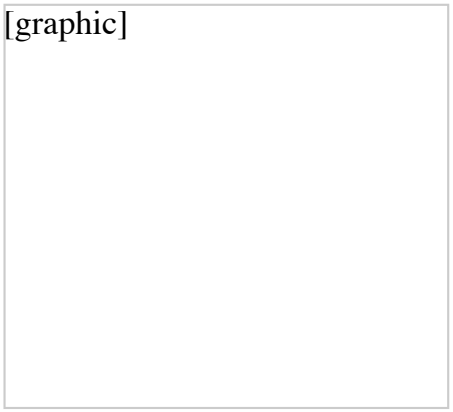

Fig. 32 Alloy AZ92A-T6 sand casting. Lamellar $Mg_{17}Al_{12}$ precipitate (light and dark gray) was produced throughout the grains of magnesium solid solution by artificial aging. Some isolated islands of Mg_2Si (white) are also present. Etchant 2, Table 1. 100×

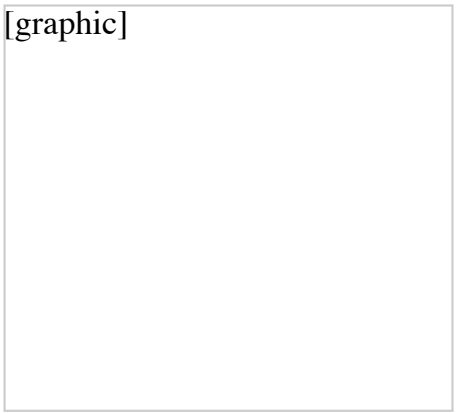

Fig. 33 Alloy AZ63A-T6 sand casting. Lamellar $Mg_{32}(Al,Zn)_{49}$ discontinuous precipitate (dark) near some grain boundaries; some particles of Mg_2Si and manganese-aluminum compounds. Note that with 6% Al there is less precipitate than with 9% Al (compare with Fig. 32). Etchant 2, Table 1, 5s. 250×

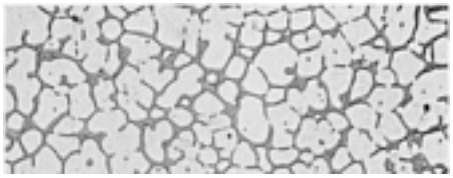

Fig. 34 EZ33A-T5 sand casting. Interdendritic network of massive Mg_9R compound. The precipitate in the dendritic grains of magnesium solid solution is not visible. Etchant 2, Table 1. 100×

[graphic]

Fig. 35 ZK51A-T5 sand casting. Fine, degenerate eutectic magnesium-zinc compound at the grain boundaries. The grains of magnesium solid solution are essentially homogeneous. Etchant 2, Table 1, 5 s. 250×

[graphic]

Fig. 36 ZH62A-T5 sand casting. Characteristic lamellar, or filigree, form of eutectic magnesium-thorium-zinc compound at the boundaries of grains of magnesium solid solution. 2% nital. 250×

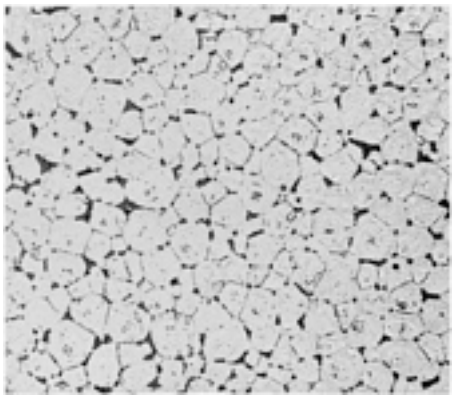

Fig. 37 QE22A-T6 sand casting. Massive Mg_9R compound is present at the boundaries of grains of

magnesium solid solution, resulting from partial solution and coalescence of the magnesium-didymium eutectic. Etchant 2, Table 1. 100×

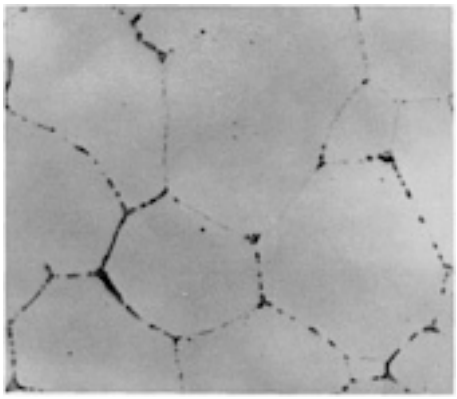

Fig. 38 HK31A-T6 sand casting. Intergranular particles of massive Mg_4Th compound (gray, outlined). The precipitate in the grains of magnesium solid solution is not visible. See Fig. 39 for effect of zinc addition. Etchant 2, Table 1, 15 s. 500×

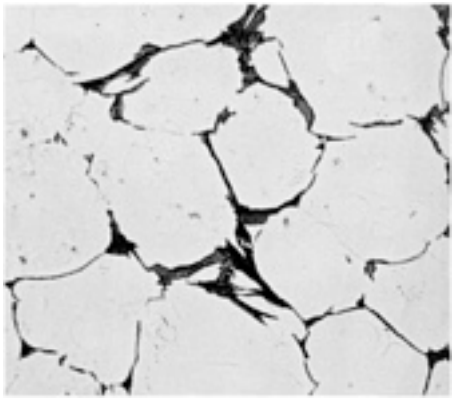

Fig. 39 HZ32A-T5 sand casting. Intergranular Mg-Th compounds: bunches of acicular compound (dark gray) and small areas of massive Mg_4Th (see Fig. 38). The precipitate within matrix grains is not visible. 2% nital. 250×

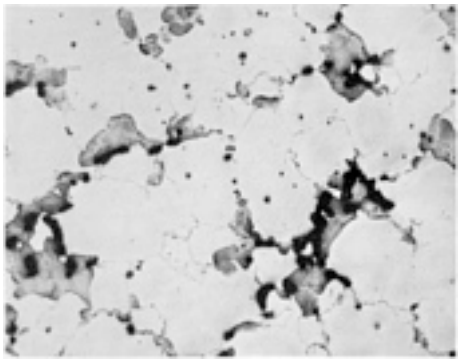

Fig. 40 Fusion microporosity in an AZ63A-T4 sand casting. Gray lamellar precipitate, present around black voids despite solution heat treatment, indicates alloy segregation in these areas. See also Fig. 41. Etchant 2, Table 1, 10 s. 100×

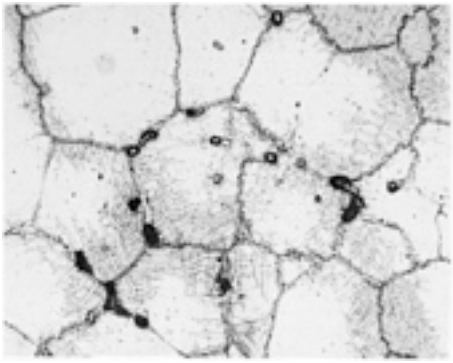

Fig. 41 Fusion microporosity in an AZ63A-T4 sand casting. The gray crackled film, formed around the black voids by the acetic-picral etchant indicates alloy segregation in these areas. See also Fig. 40. Etchant 6, Table 1, 15 s. 100×

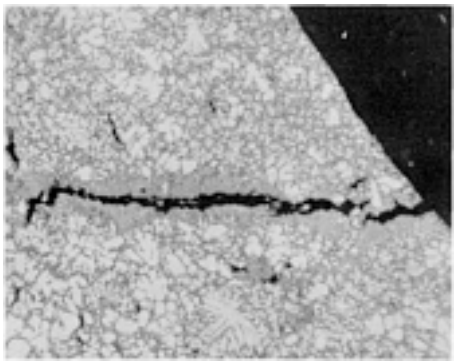

Fig. 42 Hot tear in an AZ91A-F die casting. Tear occurred in an area of compound segregation that was last to solidify and least resistant to stress caused by mold restriction during solidification shrinkage. Etchant 2, Table 1, 5 s. 75×

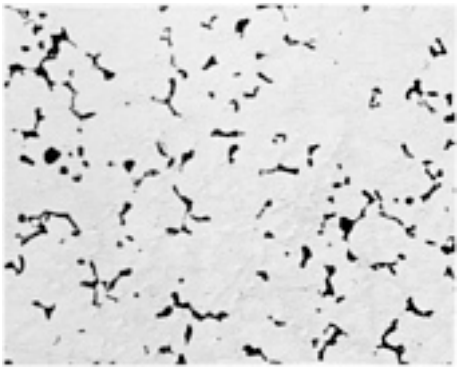

Fig. 43 Shrinkage microporosity in an AZ92A-T6 sand casting. The uniform dispersion of voids (black) in particular areas of the casting is typical of this type of porosity, which results from improper feeding of molten metal to those areas. See also Fig. 44. Etchant 2, Table 1. 100×

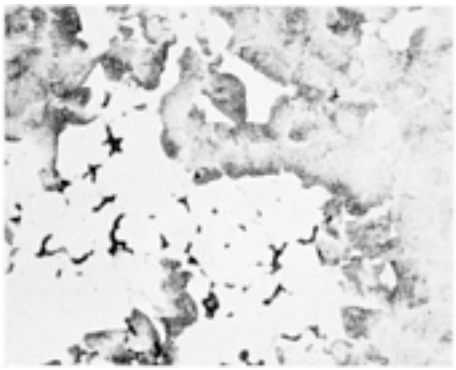

Fig. 44 Shrinkage microporosity in an AZ92A-T6 sand casting. Voids (black), resulting from

withdrawal of molten eutectic from between dendrites during solidification, are surrounded by areas low in alloying elements and containing no gray precipitate. Etchant 2, Table 1, 5 s. 100×

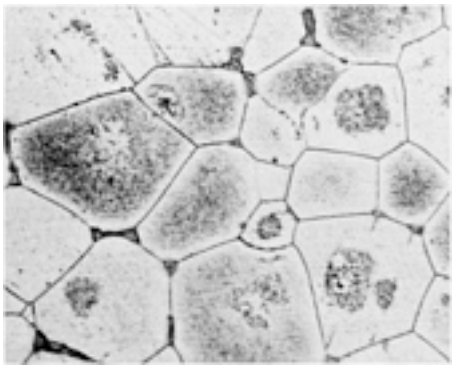

Fig. 45 QE22A-T6 sand casting. Alloy segregation (coring), characterized by intragranular precipitation of didymium and zirconium hydrides (formed during solution treatment by reaction with water vapor) and by less Mg_9R at grain boundaries than normal. Etchant 3, Table 1. 500×

[graphic]

Fig. 46 Segregation of zinc-zirconium-iron compound in a ZK61A-F sand casting. This compound and Zr_2Zn_3 form under similar conditions; the two can be distinguished by etching with 10% HF, which attacks Zr_2Zn_3 but not zinc-zirconium-iron. Etchant 2, Table 1, 10 s. 250×

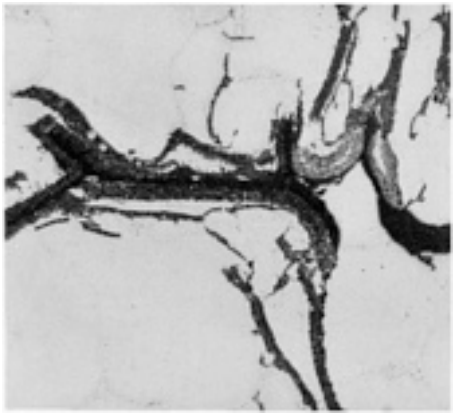

Fig. 47 Segregation of layered oxide skin in a ZK61A-F sand casting. This type of skin forms on molten metal surfaces that are incompletely protected for several minutes. Compare with the thin oxide skin shown in Fig. 48. Etchant 2, Table 1, 10 s. 250×

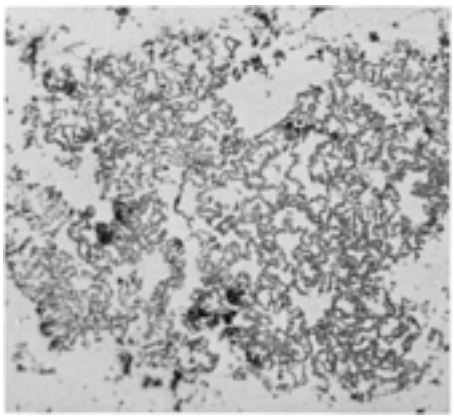

Fig. 48 Segregation of thin oxide skin in an AZ91A-F die casting. This type of skin forms whenever molten metal surfaces are exposed to the atmosphere for a few seconds. Compare with the layered oxide skin in Fig. 47. Etchant 2, Table 1, 10 s. 250×

Fig. 49 Incomplete fusion in a two-pass gas tungsten-arc butt weld in 4-mm (0.160-in.) thick AZ31B-H2A sheet. Weld was made with alloy ER AZ61A filler metal. Note the unfused area at the root of the second pass (top). Etchant 6, Table 1. 3.8×

[graphic]

Fig. 50 Shrinkage crack in the crater of a gas tungsten arc weld in an AZ92A-T6 casting caused by interruption of welding without first reducing current to lower the temperature of the weld pool. 2% nital. 75×

[graphic]

Fig. 51 Undercutting in a gas tungsten arc fillet weld in 4-mm (0.160-in.) thick AZ31B-H24 sheet.

The weld was made with ER AZ61A filler metal. Note undercut area in the edge of the top sheet of the lap joint. Etchant 6, Table 1. 3.8×

Fig. 52 Incomplete joint penetration of a gas tungsten arc weld in a butt joint between 4-mm (0.160-in.) thick AZ31B-H24 sheets. The weld was made with ER AZ61A filler metal. Note the unfused joint at the root of the weld. Etchant 6, Table 1. 3.8×

Fig. 53 Crack in the heat-affected zone of a gas tungsten arc weld in an AZ92A-T6 casting, caused by use of excessive welding current, producing too high a temperature gradient between base metal and weld pool. 2% nital. 75×

Fig. 54 Gross gas porosity in gas tungsten arc weld joining 5-mm (0.190-in.) thick AZ31B-H24 sheets; ER AZ61A filler metal. Causes include dirty base metal and filler metal, inadequate coverage by shielding gas, and moisture in gas. Etchant 6, Table 1. 3.8×

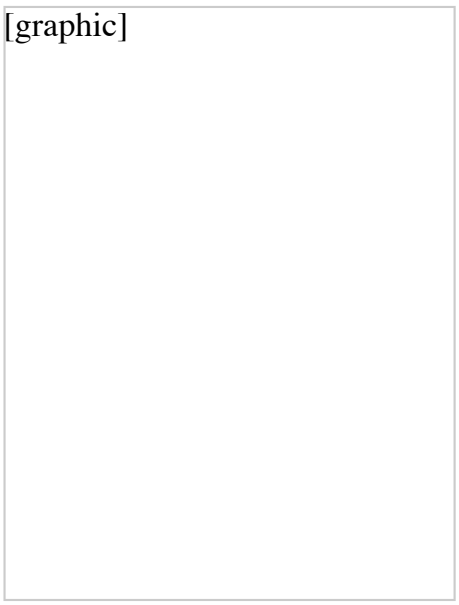

Fig. 55 Subsurface tungsten inclusion (large, round particle at top) in a gas tungsten arc weld in an

AZ92A-T6 casting. Filler metal is alloy ER AZ92A. 2% nital. 75×

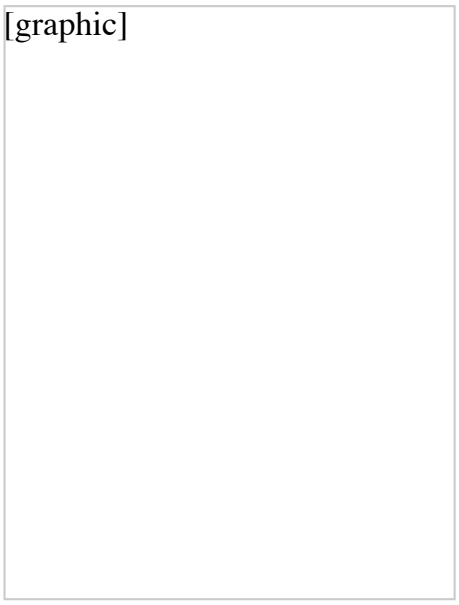

Fig. 56 Border area between zones of profuse (top) and sparse (bottom) shrinkage microporosity, in a gas tungsten arc weld deposit of ER AZ101A filler metal. Etchant 5, Table 1. 65×

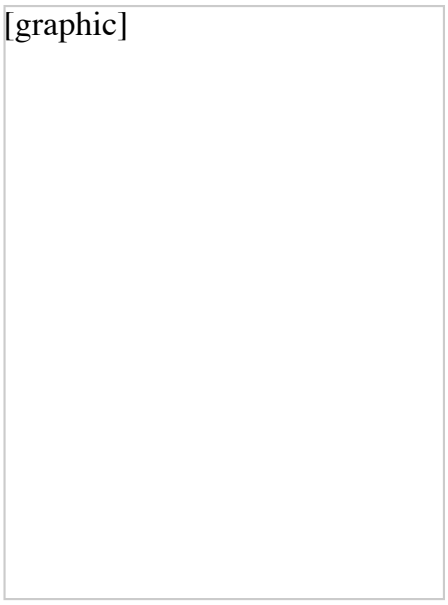

Fig. 57 Shrinkage microporosity in heat-affected zone of gas tungsten arc weld made in an AZ91C-T6 casting with ER AZ92A filler metal. (The weld deposit is at top right.) Etchant 5, Table 1. 75×

<Previous section in this article